THE ROYAL SOCIETY

The role of the mechanical system in control: a hypothesis of self-stabilization in hexapedal runners

T. M. Kubow and R. J. Full*

Department of Integrative Biology, University of California at Berkeley, Berkeley, CA 94720, USA

To explore the role of the mechanical system in control, we designed a two-dimensional, feed-forward, dynamic model of a hexapedal runner (death-head cockroach, *Blaberus discoidalis*). We chose to model many-legged, sprawled posture animals because of their remarkable stability. Since sprawled posture animals operate more in the horizontal plane than animals with upright postures, we decoupled the vertical and horizontal plane and only modelled the horizontal plane. The model was feed-forward with no equivalent of neural feedback among any of the components. The model was stable and its forward, lateral and rotational velocities were similar to that measured in the animal at its preferred velocity. It also self-stabilized to velocity perturbations. The rate of recovery depended on the type of perturbation. Recovery from rotational velocity perturbations occurred within one step, whereas recovery from lateral perturbations took multiple strides. Recovery from fore–aft velocity perturbations was the slowest. Perturbations were dynamically coupled—alterations in one velocity component necessarily perturbed the others. Perturbations altered the translation and/or rotation of the body which consequently provided 'mechanical feedback' by altering leg moment arms. Self-stabilization by the mechanical system can assist in making the neural contribution of control simpler.

Keywords: locomotion; biomechanics; insects; arthropods

1. INTRODUCTION

> 'Many researchers in neural motor control think of the nervous system as a source of commands that are issued to the body as direct orders. We believe that the mechanical system has a mind of its own, governed by the physical structure and laws of physics. Rather than issuing commands, the nervous system can only make suggestions which are reconciled with the physics of the system and task [at hand]' (Raibert & Hodgins 1993, p. 350).

Despite Raibert & Hodgins (1993) recognition that the nervous-control system, the mechanical system, and the environment all interact to determine behaviour, appeals (Chiel & Beer 1997) urging true integration are still required. In the present manuscript, we propose a simple control hypothesis for sprawled posture locomotion. We determined the extent of control offered by a feed-forward system without the benefit of feedback from the equivalent of neural reflexes. We contend that an understanding of the control algorithms potentially embedded in the mechanical system is required to define the variables controlled by the nervous system. Once control tasks are identified, then we can layer on the appropriate types of neural feedback over the control provided by the mechanical system. In the future, this approach could lead to a general control model resulting from the synthesis of feed-forward and feedback models that take advantage of the mechanical system (Schmitz *et al*. 1995; Cruse *et al*. 1996).

We chose to model sprawled posture arthropods because of their remarkable stability, simple nervous system and an increased probability that their mechanical system contributes to control. Sprawled posture animals are stable, in the vertical plane, because the height of their centre of mass is low relative to the width of their support base. As a result, sprawled posture animals can resist over-turning torques better than animals with upright postures (Alexander 1971). Sprawled posture animals with at least three legs on the ground can be statically stable during locomotion if their centre of mass falls within the tripod of support (Gray 1944; Ting *et al*. 1994).

We chose to make the model dynamic. Blickhan & Full (1987) demonstrated that rapid-running, legged arthropods must be treated as dynamic systems. Six- and eight-legged, sprawled posture animals accelerate and decelerate their bodies with each step in the same way as two- and four-legged animals do (Cavagna *et al*. 1977; Full 1989; Blickhan & Full 1993). Legged animals with both sprawled and upright postures can be modelled in the vertical plane as bouncing, spring-mass systems (Blickhan 1989; Alexander 1990; McMahon & Cheng 1990; Blickhan & Full 1993; Farley *et al*. 1993). Moreover, ghost crabs, cockroaches and ants exhibit aerial phases at fast speeds (Burrows & Hoyle 1973; Blickhan & Full 1987; Full & Tu 1991; Zollikofer 1994). The American cockroach runs on only two legs when sprinting at 50 body lengths per second (Full & Tu 1991). Most importantly, rapid-running

*Author for correspondence (rjfull@socrates.berkeley.edu).

insects can be statically unstable even when they have three legs on the ground at once (Ting *et al*. 1994). A cockroaches' centre of mass can fall outside its tripod base of support at fast speeds, yet the animal remains dynamically stable.

We chose a two-dimensional (2D), horizontal plane model for several reasons. We decoupled the model from the vertical plane because sprawled posture animals may operate primarily in the horizontal plane (Binnard 1995; Full 1997). The negative consequences of falling so close to the substrate in sprawled posture animals may be minor compared to the disruption of movement in the horizontal plane. Moreover, a whole suite of legged morphologies permit bouncing in the vertical plane. Perhaps the advantages and disadvantages of the sprawled posture morphology become more evident in the horizontal plane. Evidence for this contention comes from data on the individual-leg ground-reaction forces in cockroaches (Full *et al*. 1991). Legs generate opposing forces throughout the step period (figure 1). The zero horizontal foot force interaction criteria used in the design of some legged robots (Waldron 1986) to reduce energy expenditure is violated. The front (prothoracic) pair of legs only decelerate the insect during the stance phase, while at the same time the hind (metathoracic) pair of legs only accelerate the animal forward. The middle (mesothoracic) pair of legs first decelerate and then accelerate the body during a step. Large lateral forces have been measured (Full *et al*. 1991). Ground reaction forces tend to align along the axis of each leg, minimizing joint torque (Full *et al*. 1991; Full 1993).

Surprisingly, we discovered that the present 2D, feed-forward, dynamic, hexapod model self-stabilized to perturbations.

2. THEORETICAL MODEL

(a) *Model description and assumptions*

Our 2D, dynamic, hexaped model was anchored in the wealth of biomechanical data collected on running death-head cockroaches, *Blaberus discoidalis* (Full & Tu 1990; Full *et al*. 1991, 1995; Blickhan & Full 1993; Ting *et al*. 1994; Kram *et al*. 1997). We assumed the model to be a hexaped with a rigid body and massless legs (figure 1). Movement was constrained to the horizontal plane. This choice of plane completely removed gravity from the model. Only three degrees of freedom were permitted, two translational and one rotational. We defined the two translational degrees of freedom in two coordinate systems. In the global reference frame, we defined forward movement as positive *y*, whereas sideways movement was defined as movement along the *x*-axis (figure 2). In the reference frame of the body, fore–aft movement was in the head-to-tail direction and lateral motion was to the left or right (figure 2).

We did not include segmented legs in the model. Force inputs were single-leg ground-reaction forces acting on the body at a given foot position which stayed fixed relative to the ground for the duration of a step. The model would be underconstrained in determining joint torques and angles if we included leg segments without additional data.

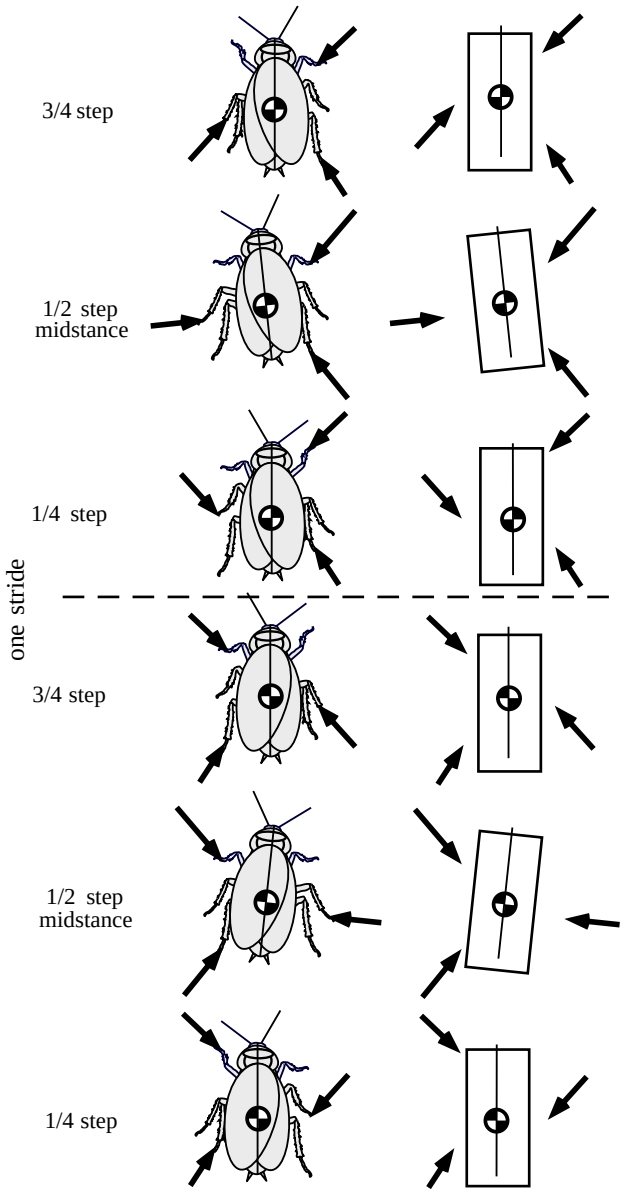

Figure 1. Two-dimensional dynamics of hexapod running. Ground-reaction forces of the legs of *Blaberus discoidalis* during one stride (Full *et al*. 1991). The front leg generates a decelerating force in the fore–aft direction, while the hind leg generates an accelerating force throughout the step period. The middle leg produces a decelerating for the first 1/2 of the step period ($t = 1/4$). The middle leg generates only a lateral force at midstance ($t = 1/2$). The middle leg produces an accelerating force during the last quarter of the step period ($t = 3/4$). The tripods are exchanged during the next step (above the dashed line). The far right column shows the simplified model we used in the present study. The rectangle represents the body and the arrows show the ground-reaction forces.

The model's control system was purely feed-forward. Explicit feedback control algorithms were not included. Leg forces were generated relative to the body using the same pattern during every step. Perturbations will undoubtedly alter leg force patterns in the animal. We contend that the response to a perturbation could consist of at least three components: (i) an active component resulting from reflexes; (ii) a passive, rapid

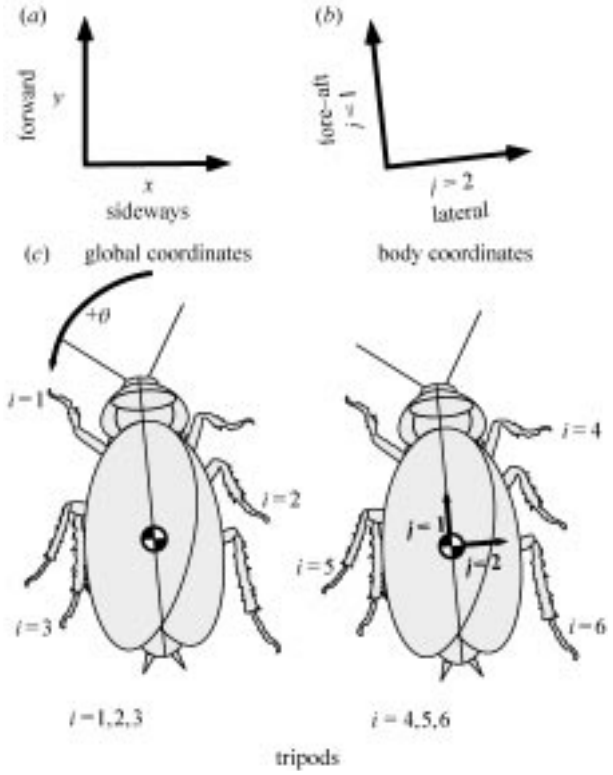

Figure 2. Coordinate system of 2D dynamic hexapod model. (*a*) x, y represent the global coordinate system where y is in the forward direction and x represents movement to the side. (*b*) j represents the coordinate system relative to the body axis where 1 is the fore–aft and 2 is the lateral axis. Positive fore–aft is towards the anterior of the animal. Positive lateral is towards the animal's right side when viewed dorsally. (*c*) For a body rotation of zero, body (fore–aft, lateral) and global (x, y) coordinate systems are the same. Legs are numbered from $i = 1$–6 (front left, middle right, back left, front right, middle left, back right, respectively).

component resulting from intrinsic musculoskeletal properties; and (iii) a passive component dependent on posture. We chose not to model all three of these components first given the lack of experimental data. To model the complete system, we argue that it is preferable to model first the stabilizing effect of posture on whole body dynamics and only then add rapid, passive and reflexive components. Given this approach, the assumption of a constant force pattern certainly demands future testing. There were no input kinematics other than the initial foot positions relative to the body at the beginning of each step, stride period, and duty factor (table 1). Stride length and the movement of the centre of mass (e.g. the three resultant velocities) were the model's outputs.

All forces were approximated as sine-wave functions. The force produced during each step by a single leg was a half sine or 180°, except for the fore–aft force of the middle leg which was a full sine-wave function. The peak of each wave used were the average maximal values recorded from the animals (table 1).

(b) *Modelling environment*

We created the model using a dynamic modelling program (Working Model 4.0, Knowledge Revolution, CA).

Table 1. *Inputs in the 2D dynamic model of the cockroach,* Blaberus discoidalis

(Leg positions are given with respect to the centre of mass as the origin.)

variable		reference
body mass (kg)	0.0025	Kram *et al*. 1997
body inertia: yaw (kg m^{-2})	2.04×10^{-7}	Kram *et al*. 1997
stride frequency (Hz)	10	Ting *et al*. 1994
duty factor	0.6[a]	Ting *et al*. 1994
leg position x, y (m)		Kram *et al*. 1997
front	± 0.011, 0.02	
middle	± 0.013, 0.007	
hind	± 0.013, -0.01	
fore–aft leg force magnitude (N)		
front	-0.0049	Full *et al*. 1991
middle	± 0.004	
hind	0.0049	
lateral leg force magnitude (N)		
front	± 0.0051	Full *et al*. 1991
middle	± 0.0051	
hind	± 0.01, 0.0032	

[a] Colour plots used to illustrate the mechanism of stabilization used a duty factor of 0.5 to simplify the calculations.

The simulation used a Kutta–Merson integrator with a variable time-step and an error of 1×10^{-5}. Time constants of stabilization were estimated by fitting velocity versus time to an exponential curve (Kaleidagraph, Synergy Software, PA). To generate plots illustrating the mechanisms behind the self-stabilization, we also implemented the model in a mathematics package (Matlab 5.1, The Mathworks, Inc., MA) for the special case of a duty factor of 0.5. We integrated with Matlab function ode23 and its default parameters (relative error of 1×10^{-3} and absolute error of 1×10^{-6}).

(c) *Model equations and symbols*

We defined the dynamic model's movement in global coordinates $(x, y$; figure 2). We refer to parameters relative to the body as fore–aft (head–tail; $j = 1$) and lateral (side-to-side; $j = 2$).

Leg force production (F) for the middle legs in the fore–aft direction was defined as

$$F_{ij} = A_{ij} \sin(2\pi s_i/k), \tag{1}$$

for $k \geqslant s \geqslant 0$ and $i = 2$, 5 and $j = 1$ where i represents a particular leg (1–6, see figure 2), j designates direction relative to the body axis (1, fore–aft and 2, lateral), A is force amplitude (N), s is the remainder of $(t + \tau - \phi_i)/\tau$, t is time (s), ϕ is phase shift relative to the left front leg, τ is stride period (s), k is the stance period (s) equal to $\tau\delta$ and δ is duty factor (see Appendix A).

Leg force production for the lateral forces of the middle legs and for the front and hind legs in both directions was defined as

$$F_{ij} = A_{ij} \sin(\pi s_i/k), \tag{2}$$

during the swing period

$$k < s < \tau, F_{ij} = 0. \tag{3}$$

The total force (TF) produced by all legs was

$$\mathrm{TF}_j = \sum_{i=1}^{6} F_{ij}. \tag{4}$$

We capitalized on the many symmetries in the motion. For example, by using an alternating tripod

$$\phi_1 = \phi_2 = \phi_3 \Rightarrow s_1 = s_2 = s_3, \tag{5}$$

$$\phi_4 = \phi_5 = \phi_6 \Rightarrow s_4 = s_5 = s_6. \tag{6}$$

Force opposition in the fore–aft force of the front and back legs allows

$$A_{11} = -A_{31}, \tag{7}$$

$$A_{41} = -A_{61}, \tag{8}$$

and lateral force opposition in the front and middle legs gives

$$A_{12} = -A_{22}, \tag{9}$$

$$A_{42} = -A_{52}. \tag{10}$$

Using these symmetries to cancel terms, we can expand the summation of equation (4)

$$F_{11} = -F_{31}, \tag{11}$$

$$F_{41} = -F_{61}, \tag{12}$$

$$\mathrm{TF}_1 = F_{21} + F_{51}(\text{middle legs}), \tag{13}$$

$$F_{12} = -F_{22}, \tag{14}$$

$$F_{42} = -F_{52}, \tag{15}$$

$$\mathrm{TF}_2 = F_{32} + F_{62}(\text{hind legs}). \tag{16}$$

Rotating to global coordinates (global positive y points anteriorly when the model has zero body rotation; global positive x points to the model's right when viewed dorsally; figure 2), the translational acceleration of the centre of mass in the y and x direction become

$$\ddot{y} = (\mathrm{TF}_1\cos(\theta) + \mathrm{TF}_2\sin(\theta))/m, \tag{17}$$

$$\ddot{x} = (\mathrm{TF}_2\cos(\theta) - \mathrm{TF}_1\sin(\theta))/m, \tag{18}$$

where θ is body rotation relative to the y-axis (positive being anticlockwise when model viewed dorsally; figure 2) and m represents body mass.

Expanding, we find that force in the y-direction is primarily due to the fore–aft force of the middle legs, but for larger rotations is influenced by the lateral force of the hind legs.

$$\begin{aligned}\ddot{y} = [&(A_{21}\sin(2\pi s_2/k) + A_{51}\sin(2\pi s_5/k)) \times \cos(\theta)\\ &+ (A_{32}\sin(\pi s_3/k) + A_{62}\sin(\pi s_6/k)) \times \sin(\theta)]/m,\end{aligned} \tag{19}$$

$$\begin{aligned}\ddot{x} = [&(A_{32}\sin(\pi s_3/k) + A_{62}\sin(\pi s_6/k)) \times \cos(\theta)\\ &- (A_{21}\sin(2\pi s_2/k) + A_{51}\sin(2\pi s_5/k)) \times \sin(\theta))]/m.\end{aligned} \tag{20}$$

Torque can be calculated from the moment arms (l) and forces in the fore–aft ($j = 1$) and lateral ($j = 2$) directions:

$$\begin{aligned}l_{il} = &(p_{i2} \times \cos(\theta(t - s_i)) - p_{i1} \times \sin(\theta(t - s_i))\\ &- x(t) + x(t - s_i)) \times \cos(\theta(t))\\ &+ (p_{i1} \times \cos(\theta(t - s_i)) + p_{i2} \times \sin(\theta(t - s_i))\\ &- y(t) + y(t - s_i)) \times \sin(\theta(t)),\end{aligned} \tag{21}$$

$$\begin{aligned}l_{i2} = &(p_{i1} \times \cos(\theta(t - s_i)) + p_{i2} \times \sin(\theta(t - s_i))\\ &- y(t) + y(t - s_i)) \times \cos(\theta(t))\\ &+ (p_{i2} \times \cos(\theta(t - s_i)) - p_{i1} \times \sin(\theta(t - s_i))\\ &- x(t) + x(t - s_i)) \times \sin(\theta(t)),\end{aligned} \tag{22}$$

where p is position at leg touchdown relative to body position along fore–aft, lateral axis and $x(t)$, $y(t)$ specify the global location of the centre of mass.

The torque for each leg is

$$T_i = (F_{i1}l_{i1} - F_{i2}l_{i2}). \tag{23}$$

The total torque (TT) is the sum for all legs

$$\mathrm{TT} = \sum_{i=1}^{6} T_i \tag{24}$$

Because of the symmetries in the force equations and the fact the body position terms are equal for the three legs of a tripod some differences in moment arm lengths become only a function of body angle change during a stride. See equations (25)–(28) in Appendix B. Most noteworthy about these equations is that the moment arm differences are unchanged by motion of the centre of mass. Equal, but opposing leg forces which cancel, allow further simplification of the torque equations

$$T_1 = -F_{31}l_{11} + F_{22}l_{12}, \tag{29}$$

$$T_2 = F_{21}l_{21} - F_{22}l_{22}, \tag{30}$$

$$T_3 = F_{31}l_{31} - F_{32}l_{32}, \tag{31}$$

$$\begin{aligned}T_1 + T_2 + T_3 = &F_{31}(l_{31} - l_{11}) + F_{22}(l_{12} - l_{22})\\ &+ F_{21}l_{21} - F_{32}l_{32},\end{aligned} \tag{32}$$

$$T_4 = -F_{61}l_{41} + F_{52}l_{42}, \tag{33}$$

$$T_5 = F_{51}l_{51} - F_{52}l_{52}, \tag{34}$$

$$T_6 = F_{61}l_{61} - F_{62}l_{62}, \tag{35}$$

$$\begin{aligned}T_4 + T_5 + T_6 = &F_{61}(l_{61} - l_{41}) + F_{52}(l_{42} - l_{52})\\ &+ F_{51}l_{51} - F_{62}l_{62}.\end{aligned} \tag{36}$$

Substituting the moment arms from equations (25)–(28), total torque (TT) becomes the sum of torque from four sources

$$\underset{\text{(fore–aft } F)}{\mathcal{T}_{\text{front+hind}}(\theta)} + \underset{\text{(lateral } F)}{\mathcal{T}_{\text{front+middle}}(\theta)} + \underset{\text{(lateral } F)}{\mathcal{T}_{\text{hind}}(\theta,y)} + \underset{\text{(fore–aft } F)}{\mathcal{T}_{\text{middle}}(\theta,x)}, \quad (37)$$

where all sources are a function of θ. $\mathcal{T}_{\text{hind}}$ is the torque most affected by changes in y, and $\mathcal{T}_{\text{middle}}$ is the torque most affected by changes in x. The forces listed in parentheses below the torques are those responsible for producing the torques. The explicit formulation of these torques are equations (B5)–(B8) in Appendix B. Fortunately, the primary components of these equations can be identified. First, $\mathcal{T}_{\text{front+hind}}(\theta)$ (equation (B5)) is primarily the magnitude of the fore–aft forces of the front or hind legs multiplied by the lateral distance between their foot placements. Second, $\mathcal{T}_{\text{front+middle}}(\theta)$ (equation (B6)) is primarily the magnitude of the lateral force of the front or middle legs multiplied by the fore–aft distance between their foot placements. Third, $\mathcal{T}_{\text{hind}}(\theta, y)$ (equation (B7)) is the torque due to the lateral force of the hind legs, and is the torque primarily affected by changes in movement along the fore–aft axis. Finally, $\mathcal{T}_{\text{middle}}(\theta, x)$ (equation (B8)) is the torque due to fore–aft force of the middle legs, and is the torque primarily affected by changes in movement along the lateral axis.

The four identifiable sources of torque are all affected by the amount of body rotation during a step. If we assume that the body rotates a small amount, so $\cos(\theta) >> \sin(\theta)$, then changes in initial fore–aft velocity primarily affect the torque created by the lateral force of the hind leg (equation (B7)) as the sine terms drop out of equation (B8) removing $y(t)$. Similarly, changes in initial lateral velocity primarily affect the torque created by the fore–aft force of the middle leg (equation (B8)) as the sine terms drop out of equation (B7) removing $x(t)$. Notice equations (B5) and (B6) have no centre of mass position terms.

3. MODEL INPUT PARAMETERS

The body mass and inertia used in the model were taken from direct measurements on the death-head cockroach, *B. discoidalis* (Kram *et al*. 1997; table 1). The stride period (τ) and duty factor (δ) were set to 100 ms and 0.6, respectively based on the data at a preferred velocity (*ca*. 25 cm s^{-1} from Full *et al*. (1991)).

Leg position at touchdown relative to body coordinates with the centre of mass as the origin was estimated from three-dimensional kinematic data available from Kram *et al*. (1997) (table 1). The assumption of massless legs appears reasonable because when totalled they only represent 6% of the body mass in cockroaches compared to 20–50% in mammals and birds (Kram *et al*. 1997). Phase shift was made relative to the left front leg. We imposed a perfect alternating tripod, such that left front, right middle, and left hind legs all had the same phase of zero. Right front, left middle, and right hind legs all had the same phase of $\tau/2$, or 180° out of phase with the other three legs forming the tripod. The magnitude of the leg ground-reaction forces were taken from direct measurements using a force platform (Full *et al*. 1991; table 1).

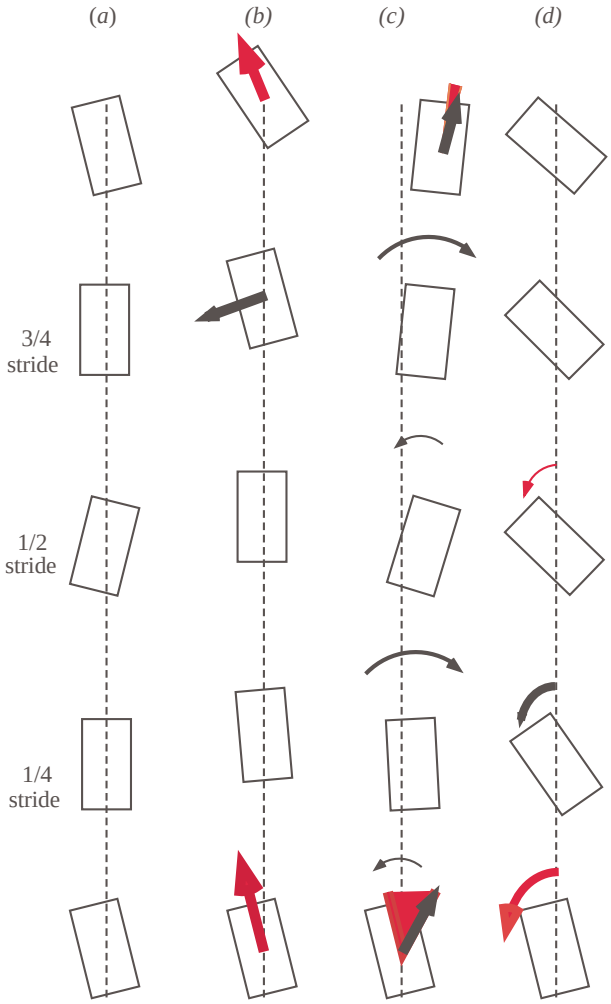

Figure 3. Kinematics of a stable stride and recovery from three perturbations. (*a*) Kinematics of a stable stride. The rectangle represents the animal's body and is moving from the bottom to top of the figure. (*b*) Recovery to a fore–aft velocity perturbation. The red arrow at the base of the column indicates an increased forward velocity. As the stride progresses, the body rotates to the left (positive) so that the lateral force (black arrow) points backwards decelerating the forward velocity towards the stable state. The amount of recovery is exaggerated to illustrate the kinematics that occur each stride to produce stabilization. (*c*) Recovery to a lateral velocity perturbation. The black arrow at the base of the column indicates the new velocity after a perturbation to the animal's right. The red angle indicates the perturbation misalignment between the new heading and the body axis created by the change in lateral velocity. The curved arrows indicate the change in torque. Notice that arrows alternate between a small change increasing misalignment of the body axis with the heading and a larger change returning the alignment to the stable state. The amount of recovery is exaggerated to illustrate the within-stride kinematics. (*d*) Recovery from a rotational velocity perturbation. The large red arrow indicates initial perturbation. As indicated by the small red arrow the perturbation is almost completely recovered from within a stride. However, the perturbation results in a body rotation that will recover in the same way as column (*c*).

There are three different types of initial state perturbations corresponding to the three degrees of freedom. We perturbed the velocity of the body independently along the fore–aft (figure 3*b*), lateral (figure 3*c*), and rotational

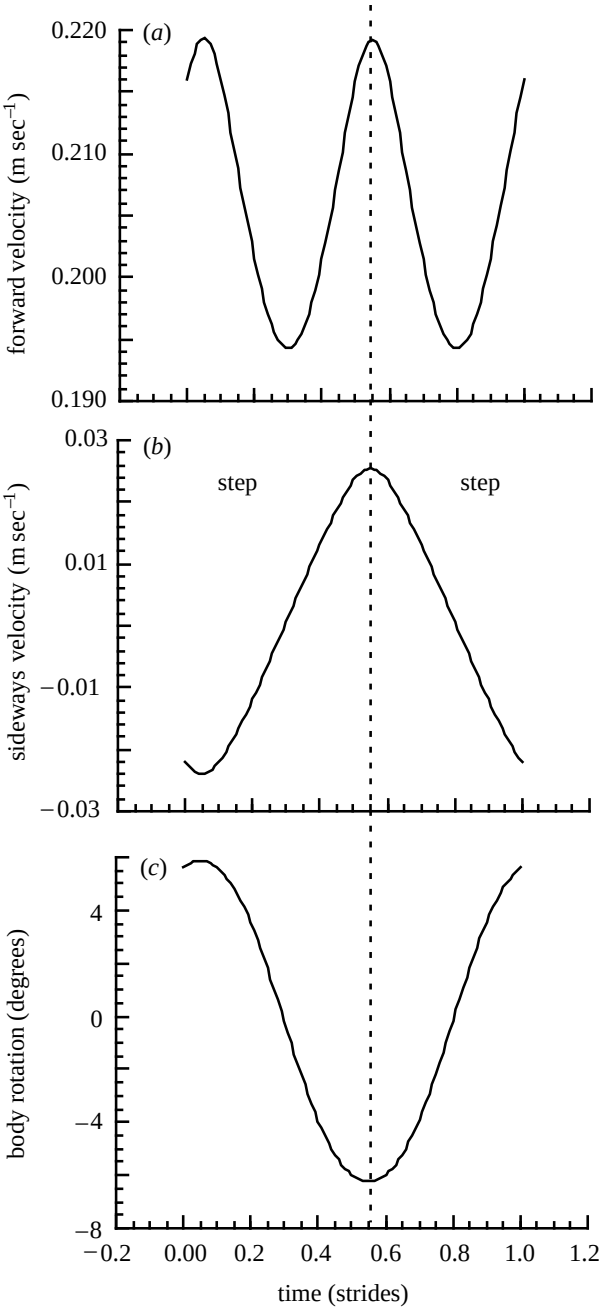

Figure 4. Model dynamics of stable running. (*a*) Forward (*y*-axis) velocity versus time. (*b*) Sideways (*x*-axis) velocity versus time. (*c*) Body rotation versus time.

(figure 3*d*) axes. Small initial rotations fore–aft and lateral perturbations are roughly equivalent to forward and sideways velocity perturbations, respectively.

4. RESULTS AND DISCUSSION

(a) *Model dynamics similar to an animal in stable state*

The mean forward velocity of the model's centre of mass was 0.21 m s^{-1} with an amplitude of oscillation of *ca.* 0.013 m s^{-1} (figure 4*a*). The mean forward velocity was similar to that measured as the preferred speed of *B. discoidalis* (Full *et al.* 1991). The variation in forward velocity was comparable to that derived from force platform measurements (Full & Tu 1990). The period of oscillation of the model's centre of mass equalled half of the stride period. A deceleration during the first half of a step was followed by an acceleration. These are the same phase relationships observed by the cockroach during running (Full & Tu 1990).

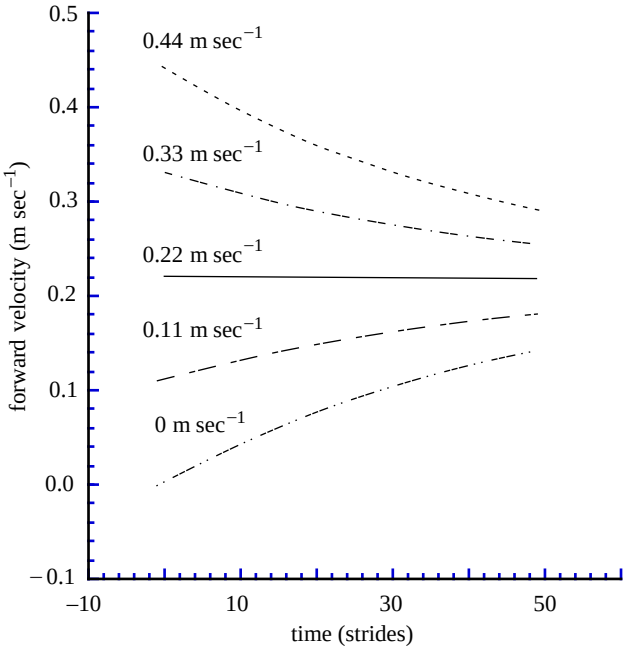

Figure 5. Recovery of forward (*y*-axis) velocity, plotted once a stride, versus time from fore–aft velocity perturbations. Perturbations represent an instantaneous change in the velocity of the centre of mass.

The sideways (*x*-axis) velocity of the model's centre of mass fluctuated with a period equal to the stride period (figure 4*b*). The mean sideways (*x*-axis) velocity was zero with an amplitude of oscillation equal to 0.026 m s^{-1}. These values were comparable to those derived from force platform measurements (Full & Tu 1990).

Body rotation fluctuated with the same period as lateral velocity with an amplitude of 12° (figure 4*c*). The pattern and magnitude of the body rotation were comparable to that measured in running animals (Kram *et al.* 1997).

(b) *Slow rate of recovery from fore–aft velocity perturbations*

We introduced a series of large, instantaneous velocity perturbations (initial fore–aft velocity = 0.00, 0.11, 0.22, 0.33, 0.44 m s^{-1}) to the model's centre of mass. The model recovered from each perturbation as a decaying exponential with nearly the same time constant (5 s; figure 5). Recovery to 63% of the stable fore–aft velocity took nearly 50 strides.

(c) *Mechanism of recovery from fore–aft velocity perturbations*

The model recovered from perturbations of fore–aft velocity because

(i) perturbing fore–aft velocity changed the distance the centre of mass travels during a step;
(ii) changes in the distance moved by the centre of mass altered the moment arm of the lateral forces produced by each leg (equation (22)). Alterations in

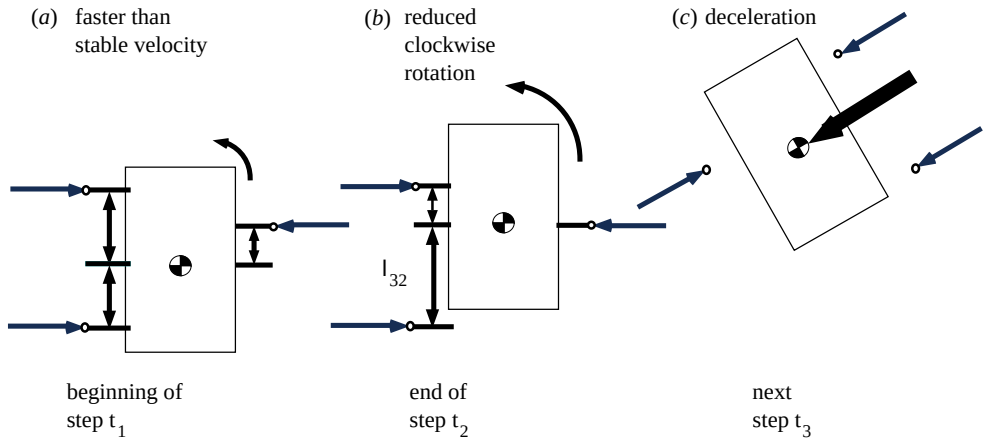

Figure 6. A spatial model representing the mechanisms of recovery from a fore–aft velocity perturbation. (*a*) Beginning of the first step (t_1). The model's centre of mass was perturbed faster than the stable velocity (i.e. $>0.3\,m\,s^{-1}$ for the 0.5 duty factor case, 0.21 normally). Single-headed arrows represent lateral forces perpendicular to the body. Double-headed arrows represent moment arms of the lateral forces. (*b*) End of the first step (t_2). The model's centre of mass moved further forward than it would at its stable velocity. The more forward position of the centre of mass increased the lateral force moment arm of the left hind leg. The increased moment arm of the hind leg decreased the initial clockwise torque and subsequently increased the anticlockwise torque. Changes in torque reduced clockwise rotation relative to the stable velocity condition. The induced phase shift resulted in a body angle of near zero at the end of the first step. (*c*) Second step (t_3). The body axis was tilted to the left during the period of the second step. This body orientation generated a deceleration of the centre of mass in the reward (*y*-axis) direction tending to stabilize the forward velocity. Large arrow represents the net lateral force relative to the body.

the moment arms of the lateral forces change torques (equation (B7));

(iii) changes in torque shifted the phase of the body angle so as to align the lateral forces with the velocity vector. The lateral force component will produce a rearward (*y*-axis) deceleration at faster than stable velocities and a forward (*y*-axis) acceleration at slower than stable velocities (equation (17)).

Consider the example in which the model's centre of mass was perturbed faster than the stable velocity (e.g. $>0.3\,m\,s^{-1}$ for the 0.5 duty factor case, 0.22 for the 0.6 duty factor case; figure 6*a*). During the first step, the model's centre of mass moved further forward than it would at its stable velocity. The more forward position of the centre of mass increased the lateral force moment arm of the left hind leg (equation (22); figure 6*b*). The increased moment arm of the hind leg decreased the initial clockwise torque and subsequently increased the anticlockwise torque (equation (B7); lighter blue followed by darker red in figure 7). These changes in torque reduced clockwise rotation relative to the stable velocity condition. The induced phase shift resulted in a body angle of near zero at the end of the first step (time = 0.05 s; figure 8). As a result, the body axis was tilted to the left during the period of the second step (figure 6*c*; positive angles in figure 8). This body orientation generated a deceleration of the centre of mass in the rearward (*y*-axis) direction (equation (17); blue in figure 8) tending to stabilize the forward velocity.

(d) *No recovery in heading from lateral velocity perturbations*

Perturbations to lateral velocity (-0.20, -0.10, 0, 0.10, $0.20\,m\,s^{-1}$) deflected the model's centre of mass and produced a change in heading. The body rotation at the beginning of each stride eventually stabilized to a new angle equal to the arctan (lateral velocity perturbation/initial fore–aft velocity) (figure 9). The time constant for aligning the body axis with the new heading was approximately 0.8 s.

(e) *Intermediate rate of recovery in lateral velocity from lateral velocity perturbations*

The model recovered from each lateral velocity perturbation as a decaying exponential with nearly the same time constant (0.8 s; figure 10). Recovery to 63% of the stable lateral velocity took approximately eight strides. Recovery from lateral velocity perturbations was more than six times faster than the recovery to a perturbation in fore–aft velocity.

(f) *Perturbations are coupled*

Single-component velocity perturbations (fore–aft, lateral or rotational) introduced at the model's centre of mass affected all of the components of velocity. The coupling was obvious when we perturbed velocity in one direction and examined the components in the other two directions. For example, when we introduced a lateral velocity perturbation, fore–aft velocity was altered (figure 11*a*). Fore–aft velocity began with no perturbation, but over the first few strides became perturbed from the steady-state velocity on the same time-course as the recovery in lateral velocity. Subsequently, fore–aft velocity recovered slowly from the lateral velocity perturbation. The time-scale for recovery was similar to that of an induced fore–aft velocity perturbation.

Coupling is best illustrated when two velocity components are plotted on a single graph. Figure 11*b* shows that a lateral velocity perturbation to the model's centre of

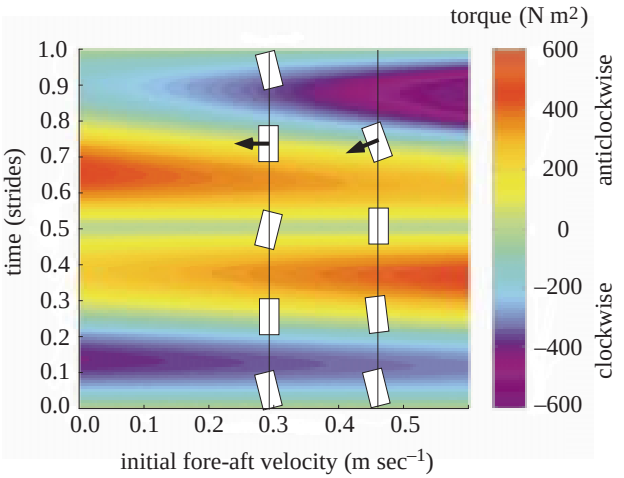

Figure 7. Absolute torque versus initial fore–aft velocity perturbation over one stride period. Torque as a function of time was calculated for a given initial fore–aft velocity. At the stable velocity (i.e. follow 0.3 m s^{-1} black line upward), torques balance resulting in only a sideways force at midstance (black arrow; 0.075 s). At a velocity faster than the stable speed (e.g. follow black line upwards at 0.45 m s^{-1}, a lateral force with a decelerating rearward (*y*-axis) component results at midstance. Deceleration results from a change in moment arms. During the first step, the increased moment arm of the hind leg decreases the initial clockwise torque (lighter blue; 0.012 s) and subsequently increases the anticlockwise torque (darker red; 0.037 s). Computed for 0.5 duty factor which is why the stable velocity is 0.30 m s^{-1}.

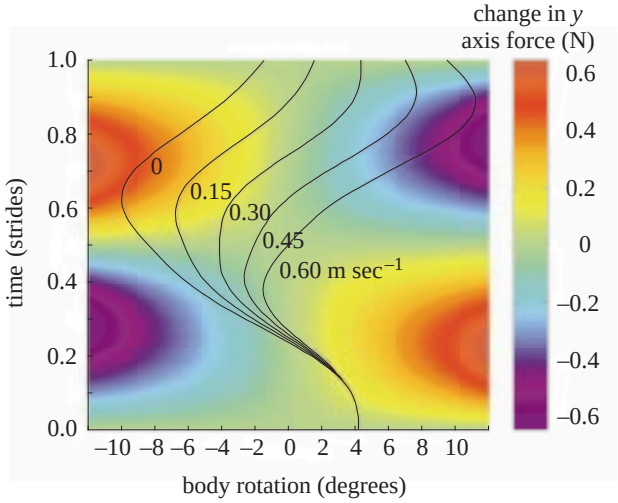

Figure 8. Change in forward (*y*-axis) force from the stable condition versus body angle for a series of fore–aft velocity perturbations over one stride period. Black lines represent the initial magnitude of fore–aft velocity. Perturbation velocities faster than the stable velocity (>0.3 m s^{-1}), produce a body rotation bias resulting in decelerating rearward (*y*-axis) forces (blue area). Perturbation velocities slower than the stable velocity, produce a body rotation bias resulting in accelerating forward (*y*-axis) forces (red area). Computed for 0.5 duty factor.

mass becomes coupled into a fore–aft velocity perturbation. The large lateral velocity perturbation (negative to the left) induced a small increase in fore–aft velocity as lateral velocity recovered. Lateral velocity recovered rapidly, whereas a fore–aft velocity recovered more slowly from its coupling-induced perturbation.

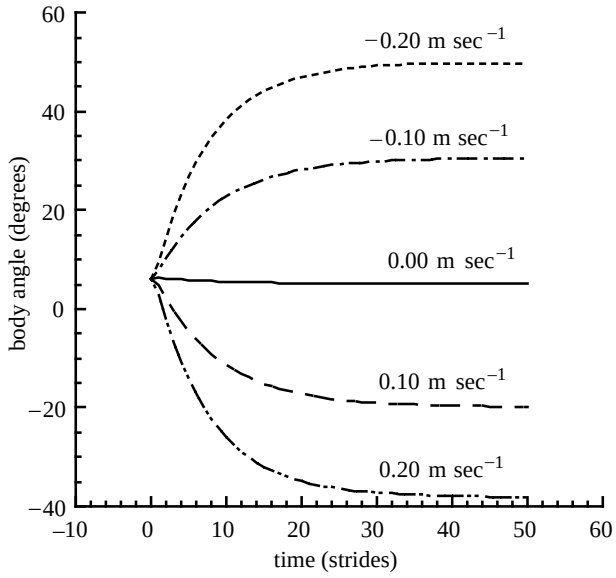

Figure 9. No recovery of the body angle, plotted once per stride, versus time from lateral velocity perturbations. Each line represents a different lateral velocity perturbation.

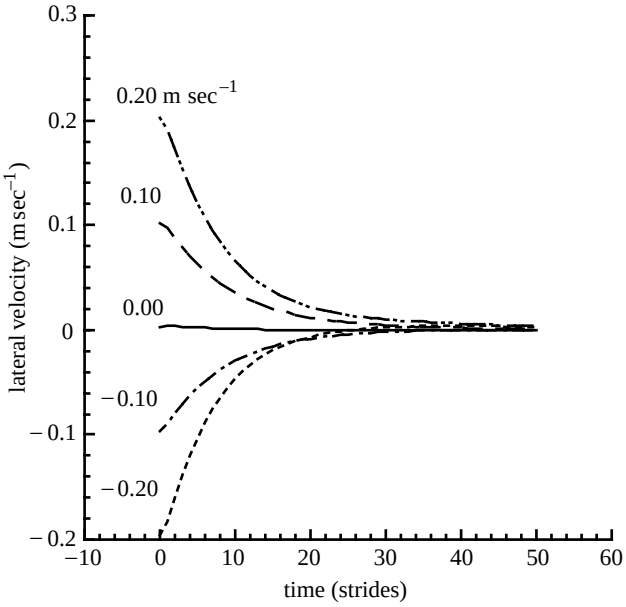

Figure 10. Recovery of lateral velocity, plotted once per stride, versus time from lateral velocity perturbations. Each line represents a different lateral velocity perturbation.

(g) *Mechanism of recovery from lateral velocity perturbations*

The model recovered from lateral velocity perturbations in two phases:

(i) the body rotated to align with the velocity vector. The velocity vector's new heading was determined by the magnitude of the lateral velocity perturbation;
(ii) after the body rotation, the lateral velocity perturbation was equivalent to a fore–aft velocity perturbation in the new heading which recovered, as described previously, for a fore–aft velocity perturbation.

Consider a lateral velocity perturbation from the left side to the model's centre of mass (positive lateral

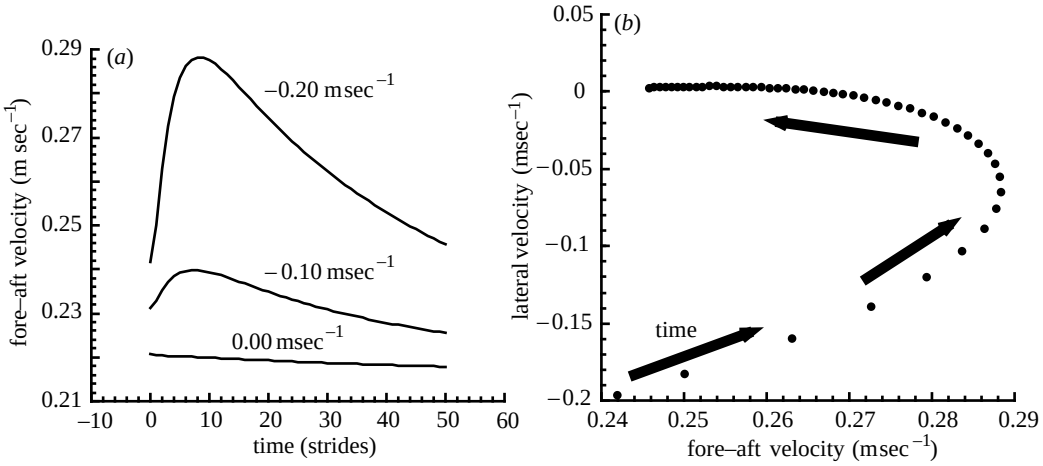

Figure 11. Dynamic coupling of the lateral velocity perturbation and fore–aft velocity. (*a*) Recovery of fore–aft velocity, plotted once per stride, versus time from lateral velocity perturbations. Each line represents a different lateral velocity perturbation. (*b*) Recovery of fore–aft and lateral velocity from lateral velocity perturbation. The lateral velocity perturbation was $-0.20\,\mathrm{m\,s^{-1}}$. Each point represents the velocities at the beginning of a stride starting in the lower left-hand corner.

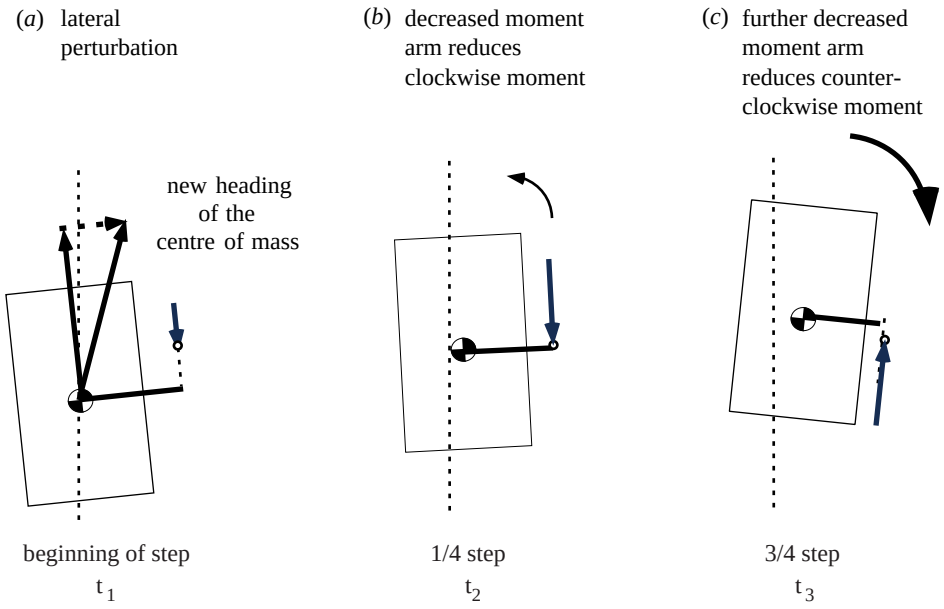

Figure 12. A spatial model representing the mechanisms of recovery from a lateral velocity perturbation. (*a*) Beginning of step (t_1). The lateral velocity perturbation from left to right alters the direction of the velocity vector and produces a new heading. The middle-leg ground-reaction force and moment arm are shown. (*b*) One-quarter of the step (t_2). The middle-leg moment arm is reduced due to the sideways (*x*-axis) movement of the centre of mass. The decreased moment arm reduces the clockwise moment. Dashed line represents the initial sideways (*x*-axis) position of the centre of mass. (*c*) Three-quarters of the step (t_3). The middle-leg moment arm is further reduced due to the sideways (*x*-axis) movement of the centre of mass. The decreased moment arm reduces the anticlockwise moment to an even greater magnitude. The reduction in anticlockwise moment tends to align the body axis with the new heading of the velocity vector.

velocity; figure 12*a*). This lateral velocity perturbation deflected the centre of mass velocity vector to the right, resulting in a new heading. During the first quarter of the step, the right middle leg generated a torque (negative, clockwise) favouring alignment of the body axis with the new heading (figure 12*b*). However, because the centre of mass had moved to the right, the moment arm of the middle leg was reduced (equation (21)). This reduction resulted in a decreased clockwise torque unfavourable to alignment with the new heading (equation (B8); lighter blue area in figure 13). During the third quarter of the step, the right middle leg generated a torque (positive, anticlockwise) opposing the alignment of the body axis with the new heading (figure 12*c*). However, because the centre of mass had moved even further to the right, the moment arm of the middle leg was greatly reduced (equation (21)). The reduced moment arm of the middle leg resulted in a greatly decreased anticlockwise torque thereby favouring alignment to the new heading (equation (B8); yellow area in figure 13).

(h) *Rapid rate of recovery from rotational velocity perturbations*

Rotational velocity exhibited the most remarkable recovery from perturbations. Rotational velocity perturbations (30,

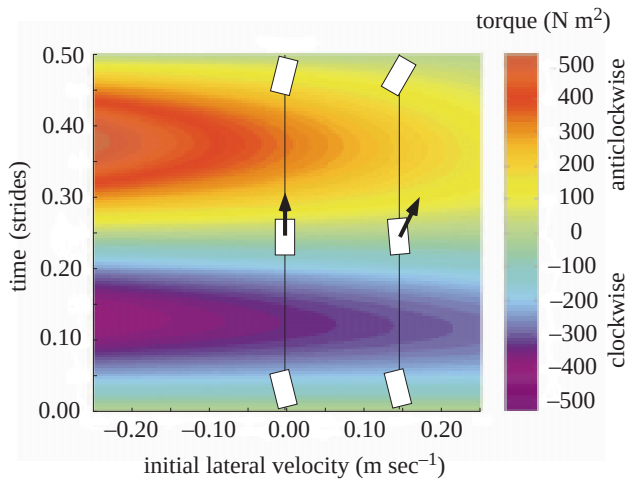

Figure 13. Torque versus initial lateral velocity perturbation over one step period. The stable velocity is shown at zero lateral velocity perturbation. A lateral velocity perturbation from left to right is shown on the right side of the figure (0.15 m s^{-1}. A reduction in the moment arm of the middle leg results in a smaller clockwise torque (lighter blue area) than in the stable state which tends to misalign the body orientation with the new velocity vector (heading of the black arrow). However, in the latter part of the step, an even greater reduction in the middle-leg moment arm reduces the anticlockwise torque (yellow area). A large reduction in anticlockwise torque tends to align the body orientation with the new velocity vector (heading). Computed for 0.5 duty factor.

15, 0, −15, −30 rad s^{-1}) converged to the stable pattern within one step period (figure 14*a*).

Interestingly, the delay in recovery of rotational velocity from a rotational velocity perturbation resulted in a misalignment of the body axis with the velocity vector. No initial perturbation in body angle was found at the beginning of the rotational velocity perturbation, but the rotation velocity perturbation subsequently turned into a body rotation which recovered more slowly than rotational velocity (figure 14*b*). The body angle perturbation recovered on the same time-scale as did a lateral velocity perturbation. The model revealed that a rotational velocity perturbation must be corrected rapidly. The greater the delay in correction, the more the body axis rotated.

(i) *Mechanism of recovery from rotational velocity perturbations*

Recovery from a rotational velocity perturbation had two phases:

(i) rotational velocity recovery—recovery from a rotational velocity perturbation resulted from individual leg force vectors changing direction so as to move out of alignment with the model's centre of mass thereby producing a correcting torque (equations (B5)–(B8));
(ii) body axis rotation and misalignment with the velocity vector corrected—the mechanism is described for the recovery to a lateral velocity perturbation.

Consider an anticlockwise rotational velocity perturbation to the model. Prior to the rotational perturbation, the force vector from, for example, the left front leg tended to be aligned through the centre of mass (figure 15*a*). After

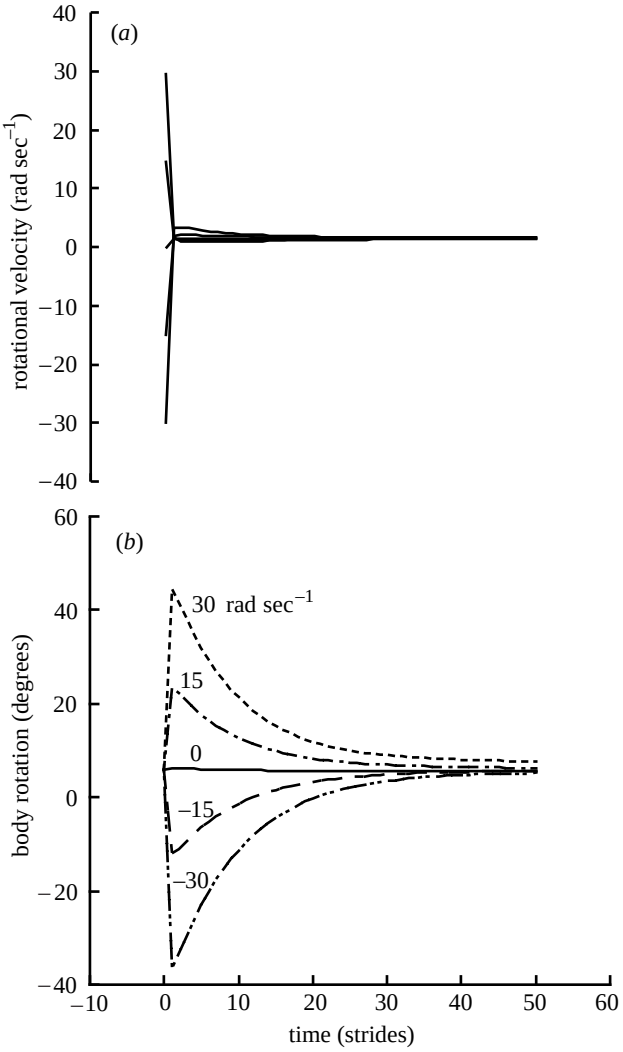

Figure 14. Recovery from rotational velocity perturbations. (*a*) Recovery of rotational velocity, plotted once per stride, from rotation velocity perturbations versus time. The rotational velocity perturbations imposed were 30, 15, 0, −15, −30 rad s^{-1}. Recovery occurred very rapidly for all rotational velocity perturbations. (*b*) Recovery of body angle, plotted once per stride, from rotation velocity perturbations versus time.

an anticlockwise rotational velocity perturbation, the rotation of the left front leg force vector resulted in a misalignment with the centre of mass thereby generating a clockwise rotational torque stabilizing the rotational velocity perturbation (figure 15*b*). Rotational velocity was stabilized within one step (constant slope of far right path at the end of one step in figure 16) due to the clockwise rotational torque (blue area in figure 16).

5. CONCLUSION

The self-stabilizing behaviour of the dynamic, feedforward hexapod model suggests an important role in control for the mechanical system. Essentially, control algorithms can be embedded in the form of the model itself. Control results from information being transmitted through mechanical arrangements. Perturbations change the translation and/or rotation of the body that consequently provide 'mechanical feedback' by altering leg moment arms

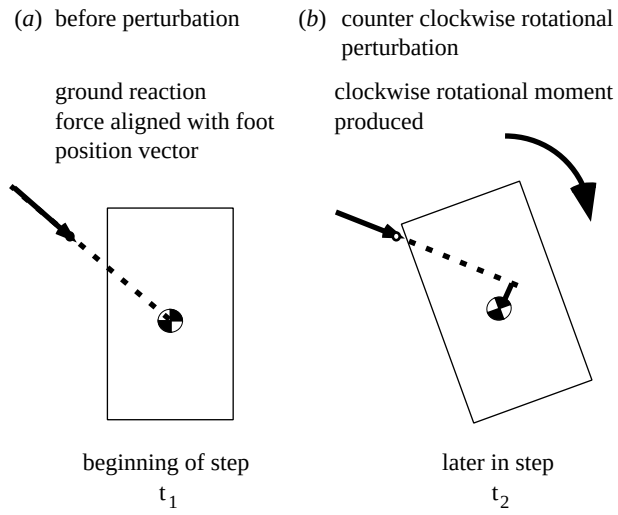

Figure 15. A spatial model representing the mechanisms of recovery from a rotational velocity perturbation. (*a*) Beginning of the step (t_1). Before a perturbation, ground-reaction forces tend to be more aligned with the centre of mass. Only small rotational torques are produced. (*b*) Later in the step (t_2). An anticlockwise rotational perturbation results in a clockwise rotational moment because the direction of ground-reaction forces rotate with the body.

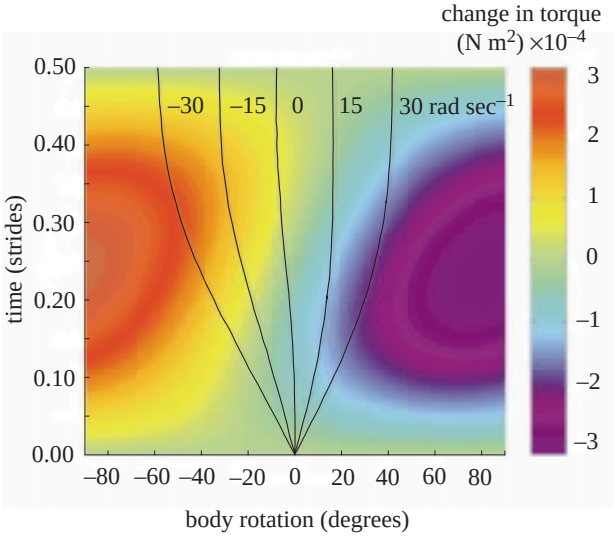

Figure 16. Change in torque from the stable condition versus body angle for rotational velocity perturbations over one step period. The rotational velocity perturbations imposed were 30, 15, 0, −15, −30 rad s^{-1}. Black lines represent rotational velocity perturbations. The slope of the lines gives rotational velocity. Rotational velocity recovers within a single step. Torque is plotted for an instantaneous change in body rotation and a duty factor of 0.5. Calculations of torque assume that the centre of mass in the fore–aft and lateral directions is not different from the stable case.

(figure 17). Even feedback-based neural models of the insect nervous system can be greatly simplified and made more adaptable when the connections of the mechanical system are exploited (Schmitz *et al*. 1995; Cruse *et al*. 1996).

The relevance of the model to sprawled posture animal locomotion requires testing the major assumptions. The assumption that foot placement occurs relative to the body after a perturbation can be determined. The variability in kinematics during constant, average velocity locomotion as well as after a perturbation must be quantified. Perhaps the most debatable assumption involved setting leg force production to be an unchanging pattern relative to the body. Certainly for extreme perturbations, it is unlikely that a leg could continue to generate the same magnitude of force in global coordinates. Moreover, it remains to be determined if the animal rotates its leg force vector with its body axis rotation. Preliminary animal experiments show that large-scale perturbations do not necessarily alter electromyographical signals of major leg muscles (Full *et al*. 1998).

However, only future animal perturbation experiments will reveal whether or not components which are stabilized rapidly in the model, such as rotational velocity (figure 14), are controlled by the behaviour of the mechanical system, whereas slow components such as fore–aft velocity (figure 5) demand neural feedback. Finally, the compromise between a simplified control system having stability in the reference frame of the body versus its loss of effectiveness in maintaining heading remains to be explored. The present model has no information about global trajectories. The heading of an animal immediately following a rapid perturbation could be directly compared to the model.

The present feed-forward model requires further development. The particular aspects of morphology and leg force production that favour self-stabilization remain unknown. Degree of sprawl, magnitude and orientation of leg forces, the effect of frequency, velocity and scaling all deserve future consideration. These parameters could be best investigated if there were a faithful analytical solution to the equations of motion.

The surprising performance of the feed-forward model has broad implications. First, the results demonstrate once again that dynamics, or the way motion evolves over time, can be important even for small, sprawled posture animals. Second, the findings encourage us to look beyond the reference frame(s) we are most familiar with. Meaningful dynamics can occur in the horizontal plane and may play a major role in manoeuvrability. Third, the model's behaviour cautions us against the assumption that continuous, proportional, negative neural feedback is sufficient. Self-stabilization by the mechanical system can assist in making the neural contribution of control simpler. The fact that the dynamics are coupled and components (fore–aft, lateral and rotation) differ in their rate of recovery from perturbations demands that we reconsider what is being controlled by the nervous system. Control strategies should work with the natural body dynamics, rather than attempting to cancel them out. Neural feedback during rapid, gross, rhythmic behaviour may play a more important role in large-scale disturbances, corrections over multiple cycles and state dependent changes.

Finally, the model reinforces the necessity to create a field of neuromechanics integrating both disciplines.

> 'It is ironic that while workers in neural motor control tend to minimize the importance of the mechanical characteristics of an animal's body, few workers in biomechanics seem very interested in the role of the nervous system. We think that the nervous system and the mechanical system should be designed to work together, sharing responsibility for the behaviour that emerges.' (Raibert & Hodgins 1993, p. 350.)

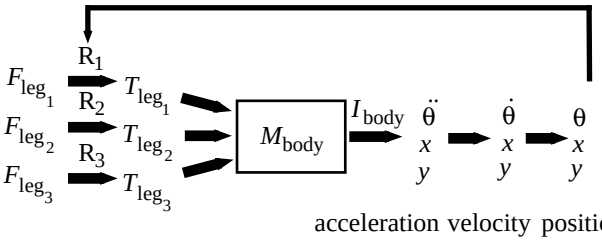

Figure 17. Feedback through the mechanical system. Leg ground-reaction forces (F) act by way of moment arms (R) to generate a torque (T). Torque on a body of a given mass (M) and inertia (I) produce a rotation (θ), sideways (x) and forward (y) translation. Feedback in this feed-forward system results from the effect of position on the moment arms.

Supported by an Office of Naval Research (ONR) Grant N00014-92-J-1250, and a Defence Advanced Research Projects Agency (DARPA) Grant N00014-98-1-0747. We thank Devin Jindrich, Phil Holmes and Johan van Leeuwen for their comments on the manuscript.

APPENDIX A

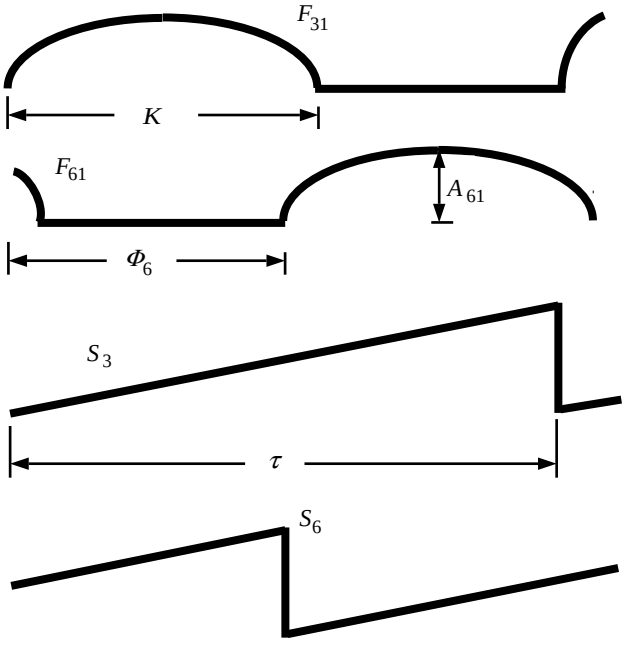

Figure A1. Model force parameters. The first trace, F_{31}, is the fore–aft ($j = 1$) force generated by the left hind leg ($i = 3$). The force lasts K seconds each step which equals the stride period (τ) times the duty factor (δ). The second trace, F_{61}, is the fore–aft force ($j = 1$) generated by the right hind leg ($i = 3$). The right hind leg has a phase shift (Φ_6) which is the time between its foot down and the foot down of the left front leg. The amplitude, A_{61}, of the force curve is positive indicating a forward acceleration. To generate a force which has a frequency different to the stride frequency, we generated a within-stride time (S_i). This goes from zero at foot down to t for each leg. Since all legs in the first tripod ($I = 1,2,3$) have a phase shift of zero, they all have a within-stride time equal to S_3. All legs in the second tripod ($i = 4,5,6$) have a phase shift equal to $\tau/2$ so the within-stride time equals S_6.

APPENDIX B

Moment arm difference equations:

$$\begin{aligned} l_{31} - l_{11} = {} & ((p_{32}\times\cos(\theta(t-s_3)) - p_{31}\times\sin(\theta(t-s_3))) \\ & -(p_{12}\times\cos(\theta(t-s_1)) - p_{11}\times\sin(\theta(t-s_1)))) \times \cos(\theta(t)) \\ & +((p_{32}\times \sin(\theta(t-s_3)) + p_{31} \times \cos(\theta(t - s_3))) \\ & -(p_{12}\times\sin(\theta(t-s_1)) + p_{11}\times\cos(\theta(t-s_1)))) \times \sin(\theta(t)), \end{aligned} \tag{B1}$$

$$\begin{aligned} l_{61} - l_{41} = {} & ((p_{62} \times \cos(\theta(t - s_6)) - p_{61} \times \sin(\theta(t - s_6))) \\ & -(p_{42}\times\cos(\theta(t-s_4)) - p_{41}\times\sin(\theta(t - s_4)))) \times\cos(\theta(t)) \\ & + ((p_{62}\times\sin(\theta(t-s_6)) + p_{61}\times\cos(\theta(t - s_6))) \\ & -(p_{42}\times\sin(\theta(t-s_4)) + p_{41}\times\cos(\theta(t-s_4)))) \times \sin(\theta(t)), \end{aligned} \tag{B2}$$

$$\begin{aligned} l_{12} - l_{22} = {} & ((p_{11} \times \cos(\theta(t - s_1)) + p_{12} \times \sin(\theta(t - s_1)) \\ & - (p_{21} \times \cos(\theta(t - s_2)) + p_{22} \times \sin(\theta(t - s_2))) \\ & \times\cos(\theta(t)) + ((p_{12}\times\cos(\theta(t - s_1)) - p_{11}\times \sin(\theta(t-s_1)) \\ & -(p_{22}\times\cos(\theta(t-s_2)) - p_{21}\times\sin(\theta(t-s_2)))\times\sin(\theta(t)), \end{aligned} \tag{B3}$$

$$\begin{aligned} l_{42} - l_{52} = {} & ((p_{41}\times\cos(\theta(t - s_4)) + p_{42} \times \sin(\theta(t - s_4)) \\ & -(p_{51}\times\cos(\theta(t - s_5)) + p_{52} \times \sin(\theta(t - s_5)))\times\cos(\theta(t)) \\ & +((p_{42}\times\cos(\theta(t - s_4)) - p_{41} \times \sin(\theta(t - s_4)) \\ & -(p_{52}\times\cos(\theta(t - s_5)) - p_{51}\times \sin(\theta(t - s_5)))\times\sin(\theta(t)). \end{aligned} \tag{B4}$$

Resultant torques from opposing leg forces:

$$\begin{aligned} T_{\text{front+hind}} = {} & F_{31}[((p_{32}\times\cos(\theta(t-s_3)) - p_{31}\times\sin(\theta(t-s_3))) \\ & -(p_{12}\times\cos(\theta(t - s_1)) - p_{11}\times\sin(\theta(t - s_1))))\times\cos(\theta(t)) \\ & +((p_{32}\times\sin(\theta(t-s_3)) + p_{31}\times\cos(\theta(t-s_3))) \\ & -(p_{12}\times \sin(\theta(t-s_1)) + p_{11}\times\cos(\theta(t - s_1))))\times\sin(\theta(t))] \\ & + F_{61}[((p_{62}\times\cos(\theta(t-s_6)) - p_{61}\times\sin(\theta(t-s_6))) \\ & -(p_{42}\times\cos(\theta(t-s_4)) - p_{41}\times\sin(\theta(t-s_4))))\times\cos(\theta(t)) \\ & +((p_{62}\times\sin(\theta(t-s_6)) + p_{61}\times\cos(\theta(t-s_6))) \\ & -(p_{42}\times\sin(\theta(t-s_4)) + p_{41}\times\cos(\theta(t-s_4))))\times\sin(\theta(t))], \end{aligned} \tag{B5}$$

$$\begin{aligned} T_{\text{front+middle}} = {} & F_{22}[((p_{11}\times\cos(\theta(t-s_1)) + p_{12}\times\sin(\theta(t-s_1)) \\ & -(p_{21}\times\cos(\theta(t-s_2)) + p_{22}\times\sin(\theta(t-s_2)))\times\cos(\theta(t)) \\ & + ((p_{12}\times\cos(\theta(t-s_1)) - p_{11}\times\sin(\theta(t-s_1)) \\ & -(p_{22}\times\cos(\theta(t-s_2)) - p_{21}\times\sin(\theta(t-s_2)))\times\sin(\theta(t))] \\ & + F_{52}[((p_{41}\times\cos(\theta(t-s_4)) + p_{42}\times\sin(\theta(t-s_4)) \\ & -(p_{51}\times\cos(\theta(t-s_5)) + p_{52}\times\sin(\theta(t-s_5)))\times\cos(\theta(t)) \\ & +((p_{42}\times\cos(\theta(t-s_4)) - p_{41}\times\sin(\theta(t-s_4)) \\ & -(p_{52}\times\cos(\theta(t-s_5)) - p_{51}\times\sin(\theta(t-s_5)))\times\sin(\theta(t))], \end{aligned} \tag{B6}$$

$$\begin{aligned} T_{\text{hind}} = {} & -F_{32}[(p_{31} \times \cos(\theta(t - s_3)) + p_{32} \times \sin(\theta(t - s_3)) \\ & -y(t) + y(t - s_3) \times \cos(\theta(t)) \\ & + (p_{32} \times \cos(\theta(t - s_3)) - p_{31} \times \sin(\theta(t - s_3)) \\ & - x(t) + x(t - s_3)) \times \sin(\theta(t))] \\ & - F_{62}[(p_{61} \times \cos(\theta(t - s_6)) + p_{62} \times \sin(\theta(t - s_6)) \\ & -y(t) + y(t - s_6)) \times \cos(\theta(t)) \\ & + (p_{62} \times \cos(\theta(t - s_6)) - p_{61} \times \sin(\theta(t - s_6)) \\ & - x(t) + x(t - s_6)) \times \sin(\theta(t))], \end{aligned} \tag{B7}$$

$$\begin{aligned} T_{\text{middle}} = {} & F_{21}[(p_{22} \times \cos(\theta(t - s_2)) - p_{21} \times \sin(\theta(t - s_2)) \\ & - x(t) + x(t - s_2)) \times \cos(\theta(t)) \\ & + (p_{21} \times \cos(\theta(t - s_2)) + p_{22} \times \sin(\theta(t - s_2)) \\ & -y(t) + y(t - s_2)) \times \sin(\theta(t))] \\ & + F_{51}[(p_{52} \times \cos(\theta(t - s_5)) - p_{51} \times \sin(\theta(t - s_5)) \\ & - x(t) + x(t - s_5)) \times \cos(\theta(t)) \\ & + (p_{51} \times \cos(\theta(t - s_5)) + p_{52} \times \sin(\theta(t - s_5)) \\ & -y(t) + y(t - s_5)) \times \sin(\theta(t))]. \end{aligned} \tag{B8}$$

REFERENCES

Alexander, R. McN. 1971 *Size and shape*. London: Edward Arnold.

Alexander, R. McN. 1990 Three uses for springs in legged locomotion. *Int. J. Robot. Res.* **9**, 53–61.

Binnard, M. B. 1995 *Design for a small pneumatic walking robot*. Cambridge, MA: MIT Press.

Blickhan, R. 1989 The spring-mass model for running and hopping. *J. Biomech.* **22**, 1217–1227.

Blickhan, R. & Full, R. J. 1987 Locomotion energetics of the ghost crab. II. Mechanics of the center of mass during walking and running. *J. Exp. Biol.* **130**, 155–174.

Blickhan, R. & Full, R. J. 1993 Similarity in multilegged locomotion: bouncing like a monopode. *J. Comp. Physiol.* A **173**, 509–517.

Burrows, M. & Hoyle, G. 1973 The mechanism of rapid running in the ghost crab, *Ocypode ceratophthalma*. *J. Exp. Biol.* **58**, 327–349.

Cavagna, G. A., Heglund, N. C. & Taylor, C. R. 1977 Mechanical work in terrestrial locomotion: two basic mechanisms for minimizing energy expenditure. *Am. J. Physiol.* **233**, R243–R261.

Chiel, H. J. & Beer, R. D. 1997 The brain has a body: adaptive behavior emerges from interactions of nervous system, body and environment. *Trends Neurosci.* **20**, 553–557.

Cruse, H., Bartling, C., Dean, J., Kindermann, T., Schmitz, J., Schumm, M. & Wagner, H. 1996 Coordination in a six-legged walking system. Simple solutions to complex problems by exploitation of physical properties. In *Proceedings of the Fourth International Conference on simulation of adaptive behaviour from animals to animats* (ed. P. Maes, M. J. Mataric, J. A. Meyer, J. Pollack & S. W. Wilson), pp. 84–93. North Falmouth, MA: MIT Press.

Farley, C. T., Glasheen, J. & McMahon, T. A. 1993 Running springs: speed and animal size. *J. Exp. Biol.* **185**, 71–86.

Full, R. J. 1989 *Mechanics and energetics of terrestrial locomotion: from bipeds to polypeds*. Innsbruck: Georg Thieme Verlag.

Full, R. J. 1993 Integration of individual leg dynamics with whole body movement in arthropod locomotion. In *Biological neural networks in invertebrate neuroethology and robotics* (ed. R. D. Beer, R. E. Ritzmann & T. McKenna), pp. 3–20. Boston, MA: Academic Press.

Full, R. J. 1997 Invertebrate locomotor systems. In: *The handbook of comparative physiology* (ed. W. Dantzler), pp. 853–930. Oxford University Press.

Full, R. J. & Tu, M. S. 1990 The mechanics of six-legged runners. *J. Exp. Biol.* **148**, 129–146.

Full, R. J. & Tu, M. S. 1991 Mechanics of a rapid running insect: two-, four- and six-legged locomotion. *J. Exp. Biol.* **156**, 215–231.

Full, R. J., Blickhan, R. & Ting, L. H. 1991 Leg design in hexapedal runners. *J. Exp. Biol.* **158**, 369–390.

Full, R. J., Yamauchi, A. & Jindrich, D. L. 1995 Single leg force production: cockroaches righting and running on photoelastic gelatin. *J. Exp. Biol.* **198**, 2441–2452.

Full, R. J., Autumn, K., Chung, J. I. & Ahn, A. 1998 Rapid negotiation of rough terrain by the death-head cockroach. *Amer. Zool.* **38**, 81A.

Gray, J. 1944 Studies in the mechanics of the tetrapod skeleton. *J. Exp. Biol.* **20**, 88–116.

Kram, R., Wong, B. & Full, R. J. 1997 Three dimensional kinematics and limb kinetic energies of running cockroaches. *J. Exp. Biol.* **200**, 1919–1929.

McMahon, T. A. & Cheng, G. C. 1990 The mechanics of running: how does stiffness couple with speed? *J. Biomech.* **23**, 65–78.

Raibert, M. H. & Hodgins, J. A. 1993 Legged robots. In *Biological neural networks in invertebrate neuroethology and robotics* (ed. R. Beer, R. Ritzmann & T. McKenna), pp. 319–354. Boston, MA: Academic Press.

Schmitz, J., Bartling, C., Brunn, D. E., Cruse, H., Dean, J., Kindermann, T., Schumm, M. & Wagner, H. 1995 Adaptive properties of hard-wired neuronal systems. *Verh. Dtsch. Zool. Ges.* **88**, 165–179.

Ting, L. H., Blickhan, R. & Full, R. J. 1994 Dynamic and static stability in hexapedal runners. *J. Exp. Biol.* **197**, 251–269.

Waldron, K. J. 1986 Force and motion management in legged locomotion. *IEEE J. Robot. Auto.* **RA-2**, 214–220.

Zollikofer, C. P. 1994 Stepping patterns in ants. I. Influence of speed and curvature. *J. Exp. Biol.* **192**, 95–106.